A Modular Framework to Predict Alzheimer's Disease Progression Using Conditional Generative Adversarial Networks

Shoumik Roychowdhury
Westwood High School
12400 Mellow Meadow Drive,
Austin, Texas 78750, USA
Email: shoumikitu@gmail.com

Shounak Roychowdhury
Department of Computer Science
Texas State University
San Marcos, TX
Email: s_r546@txstate.edu

***Abstract*—Alzheimer's disease (AD) is a chronic neurodegenerative disease that worsens over time. The number of AD cases is growing, around 3 million new US cases each year. Although state-of-the-art research shows promise, predicting the disease's rate of progression for a case by case basis remains a challenging problem. Current methods of predicting the progression of AD can delay treatment and lead to misdiagnosis. We propose a novel approach to simulate the rate of progression of AD and the atrophy of the brain over time. We seek to achieve this by generating synthetic magnetic resonance (MR) images via a series of Conditional Deep Convolutional Generative Adversarial Neural Networks (CDCGANs) and then analyze them by computing the fractal dimensionality of the cortical brain ribbons. This paper shows the feasibility of this proposal by cascading CDCGANs that simulate different stages of AD. It is possible to extend by a tandem of CDCGANs that would simulate the different stages of the disease. MR images used here are from ADNI(Alzheimer's Disease Neuroimaging Initiative). The atrophy is measure using fractal dimension (box-counting method)of the cortical ribbon(CR). A decreasing fractal dimension is a confirmation that the disease progress over time.**

I. Introduction

Alzheimer's disease (AD) is an irreversible neurodegenerative disease that progresses with time. Its main characteristics are the accumulation of a large number of amyloid plaques and neurofibrillary tangles in the brain. These plaques and tangles destroy the neurons that cause a loss of neurological faculties. Thus, cognitively, it affects memory, thinking, and social behavior. AD is the most common form of dementia. Approximately 5.7 million Americans are living with AD in 2018 [1]. The projection is that this number will rise to nearly 14 million. Unfortunately, there is no cure for this disease at the moment. Current treatments only can decelerate the progression of AD. Therefore, it is of utmost importance for timely treatment so that it possible to delay the progression. It has become clear that it is imperative to develop strategies for the detection of AD at an early stage. During its early stages, it is quite challenging to detect because cognitive faculties do not reveal the effects of subtle neural degeneration that is already underway. Over the years, researchers have identified a few categories in the AD spectrum, starting from not having the disease to the last stages of AD. This mid-range category is called Mild Cognitive Impairment (MCI), where the various degrees of cognitive impairments become noticeable. There are two main categories: NC-MCI (non-convertors) and c-MCI (converters). The c-MCI group is most at risk of transit to AD in later stages of the lives. Early detection at the MCI stages, through macro biomarkers such as isolate systolic hypertension [7], can delay the onset of the disease, before irreversible damage develops. Thus, the detection of this disease early on is an essential step towards prevention. Various studies report that MCI patients progress to AD at a rate of 10% to 15% per year, and 80% of these MCI patients will have converted to AD after approximately six years of follow-up [19].

Many studies have different types of machine learning techniques have used in the classification of AD and MCI. In the traditional machine learning setup, before the popularity of deep neural networks, Support vector machine (SVM) is a primary tool that dominated AD research for addressing the classification/regression problem. Typically, these methods use MRI, FDG-PET, and CSF data and perform a multi-task feature selection and, after that, perform regression or classification using SVM. A study reported by Zhang et al. shows 73.9% classification accuracy [23].

In a domain transfer learning technique, for MCI conversion prediction, use data from both the target domain (i.e., MCI) and other non-target domains such as AD and NC from different imaging modalities to separate MCI-C and MCI-NC patients. The results show the classification of MCI-C patients from MCI-NC patients with an accuracy of 79.4% [4]. Zhang et al. used Bayesian methods to multimodal classifying AD and MCI [22].

Cho et al. use cortex thickness as a discriminatory feature for classification. Their method uses eigenfunctions of the Laplace–Beltrami operator, which are derived from the graphical geometry of a cortical surface [5]. Cortical surface thickness is also used in the fractal analysis of cortical ribbons CR to discriminate different degrees of cerebral atrophy that occurs in Alzheimer's disease [12].

978-1-7281-6926-2/20/$31.00 ©2020 IEEE

Longitudinal studies analyze targeted spatial structures such as the hippocampus etc. to study spatial abnormalities in those structures and track it over a period of time. The longitudinal features such as bio-markers like CSF and cognitive performance are typically used in these kinds of studies [17], [16]. Zhang et al. use the SVM classifier by adding landmarks to identify the changes that in their longitudinal study [23].

The success of deep learning comes from having a massive data set that trains the system for higher accuracy, but getting labeled data set is expensive. Simonyan and Andrew investigate the effect of the depth of the Convolutional Neural Network (CNN) and its accuracy. Their study shows the effectiveness of deep layers based on large-scale image recognition data set (ImageNet Challenge 2014) [21]. The main power of CNN lies in its deep architecture, which allows the extraction of discriminating features at multiple levels of abstraction.

In 2014, Goodfellow et al. introduced a novel idea of a class of unsupervised learning technique known as Generative Adversarial Network (GAN) [8]. Since then, it has become a new paradigm of generating fake (unlabeled) data that follows the same statistical distribution of the training data. This technique has become popular for data augmentation [3] and, in general, for natural images and face-based recognition. Specifically, this is also being employed by the medical imaging community for creating fake tumors [9], lesions [6] etc. Kazuhiro et al. proposes the use of DCGAN (Deep Convolutional GAN), for the creation of realistic artificial MRI images for data augmentation and they assert that their synthetically generated data passed the examination of a group of radiologists and neurologists [11].

To predict MCI to AD conversion, we propose a novel framework that uses cascaded conditional generative neural networks to predict possible stages of MCI to AD conversion by simulating possible brain stages. We are not aware of any work that uses cascaded CDCGANs to show different stages. We discuss the details of this architecture in Section IV. Our work uses the concepts from longitudinal studies and generative adversarial network models to predict the stages of AD.

II. Conditional Generative Adversarial Network

In 2014, Goodfellow et al. introduced a novel idea of a class of unsupervised learning technique known as Generative Adversarial Network (GAN) [8]. Since then, it has become a new paradigm of generating fake (unlabeled) data that follows the same statistical distribution of the training data. GAN consists of two adversarial models: 1) a generative model (G) that samples capture the data distribution, and 2) the discriminative model (D) estimates the probability of sample (x) that it has come from the training set, which is labeled. The intention of the generator G is to construct a probability distribution p_g for a data x. It does by mapping a noise distribution $p_z(z)$ to a data space $G(x;\theta_d)$. On the other hand, the discriminator, $D(x;\theta_d)$, generates a single scalar value. This value measures the probability that x came from the training set instead of the generated distribution of p_g. Both the generator and discriminator are trained simultaneously. Thus that the generator tries to update its weights in order to minimize the generative error $log(1-D(G(z)))$. At the same time, the discriminator D tries to update its weights in order to maximize the output of $log(D(x))$. This concurrent training of G and D is like a game-theoretic strategy of minimax with value function $V(G,D)$, which is given below:

$$\min_G \max_D V(G,D) = E_{x\sim p_{data}} logD(x) + \mathbb{E}_{z\sim p_z}(z)[log(1-D(G(z)))] \quad (1)$$

Mirza and Osindero extended a conditional version of GAN termed conditional generative adversarial network [20] and it is also known as CGAN. To construct a CGAN, we need to supply an additional amount of information, y, which serves as a source of condition to both the generator and the discriminator. The following objective function for a two-player strategy.

$$\min_G \max_D V(G,D) = E_{x\sim p_{data}} logD(x|y) + \mathbb{E}_{z\sim p_z(z)}[log(1-D(G(z|y)))] \quad (2)$$

Several popular [14] and academic works [8] have use the MNIST data set to show the efficacy of the CGAN. A user provides a class label and the generator uses that class label as a condition to create an image that possibly belongs to that class label.

III. Fractal Dimension

Objects in Euclidean geometry uses integer dimensions such as points in 1-dimension, lines in 2-dimensions, planes in 3-dimensions, and so on. However, there are objects which are inherently self-similar and are expressed in fractional dimensions. Such objects are called Fractals. For example, some of the well-known fractals are Koch's snowflake or Siepenski triangle that have dimensions between 1 and 2. This means that at any aggregation a portion of the object would seem identical in structure to the entirety of the object. This self-similarity can be measured thorough fractal dimension. In this paper we will use fractal dimensions to measure deterioration of cortical ribbons.

Mandelbrot developed the fractal theory [18] to describe specific objects correctly because the complexity of certain objects cannot be adequately described by either Euclidean or topological dimensions as mentioned earlier. His work was built upon the foundations laid by mathematicians Hausdorff and Besicovitch. Box Counting [13] is a technique used to approximate the fractal dimension of an image. Initially a grid having squares of side length r is overlaid on an object. The squares that contain any portion of the object are counted and rest are discarded. This process is repeated where r is increased by a given constant.

The fractal dimension computed by the box counting [13] method is defined as follows:

$$D_H = \lim_{r\to 0^+} \frac{lnN}{ln(\frac{1}{r})}, \quad (3)$$

978-1-7281-6926-2/20/$31.00 ©2020 IEEE

where r=length of the box, and N = number of boxes.

This useful technique is used in texture segmentation, shape classification, and graphic analysis in many fields [15]. We use the Box Counting Method on binary images. Fig. 1

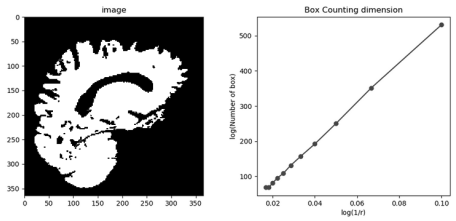

Fig. 1: Box counting technique on a MR image.

A. Multifractal

Any systems that has more than one fractal dimension is considered as a Multifractal [10]. Typically a multifractal is understood in terms of a spectrum of fractional dimensions. The brain is a multifractal body. Each two dimensional slice can be considered a fractal system as each slice holds white matter and grey matter. Thus each image is a bi-fractal because it has two fractal dimensions resulting from the white matter image and the grey matter image. Fig. 2 shows the spectrum of three normal people and three MCI patients. The yellow graph shows the fractality of the white matter and blue line shows the fractality of the gray matter.

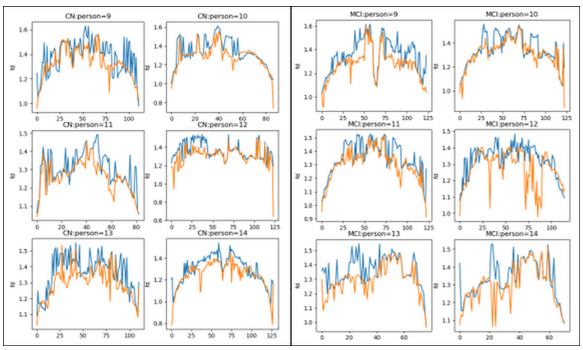

Fig. 2: This figure shows fractality of the brain of three normal persons and three MCI patients.

IV. Proposed Framework

In this section we propose our multistage framework.

A. Overview

In this paper, we propose a modular framework for predicting stages of AD. Fig. 3 shows how the series of cascaded Conditional Deep Generative Adversarial Network (CDCGAN)s work. An MR image of the patient is provided to a CDCGAN, and the network generates an image of the lossy cortical ribbon. The generated image predicts the loss of matter in specific areas of the cortical ribbon. We use the fractal dimension to quantify the amount of loss of matter in the cortical ribbon. We calculate the fractal dimension of the

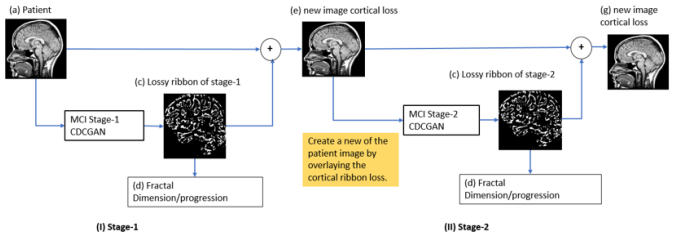

Fig. 3: This figure shows the modular design of prediction of different stages of MCI and the loss of brain matter is noted through the decline of fractal dimensions. In this figure we only show two modules, otherwise we can add as many modules as needed.

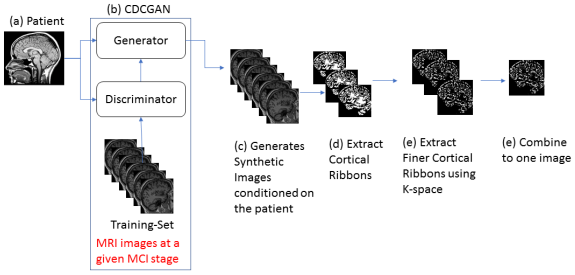

Fig. 4: Proposed design of the generated cortical ribbon that acts as a mask. This mask can be controlled by manipulating the k-space of the image.

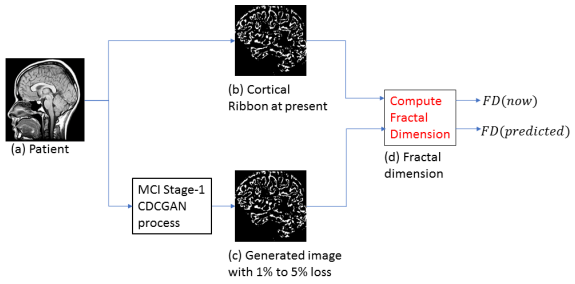

Fig. 5: Compare the fractional dimensions of the cortical ribbon of the patient's current brain image and predicted cortical ribbon that is generated the MCI images.

generated image and compare it to the fractal dimension of the original image. The input for the next CDCGAN consists of the generated image - of the lossy cortical ribbon - combined with the original MR image. This entire process is repeated for the next CDCGAN in the series of CDCGANs.

Fig. 4 demonstrates and expands on how the lossy cortical ribbon is generated. The CDCGAN trains on MR images accessed from ADNI, which is dependent on the visit time of the patient (e.g., 6 months 12 months...) while still being conditioned on the MR image of the patient. After training the CDCGAN for a substantial set of epochs, the CDCGAN generates many realistic images of brains, including the skull and other tissues similar to the patient's MRI.

The extracted cortical ribbon images are noisy. By removing

978-1-7281-6926-2/20/$31.00 ©2020 IEEE

the high frequencies of the image, we are able to retain the core structures of the cortical ribbon, while removing noise. Therefore, we are interested in finding the low-frequency information embedded within the generated images. To distill all of the low-frequency images, we employ the k-space (2d-Fourier transform). The k-space of each image is then processed and modified by under-sampling, explicitly by preserving the central portion of the k-space. Reconstruction of the manipulated k-space results in a clear MR image that captures the core structures of the cortical ribbons. We then overlay the new reconstructed images by computing the mean of the images, resulting in the formation of one final image. This final image embodies a statistical representation that consists of possibly standard features that are retained by MCI patients.

B. CDCGAN

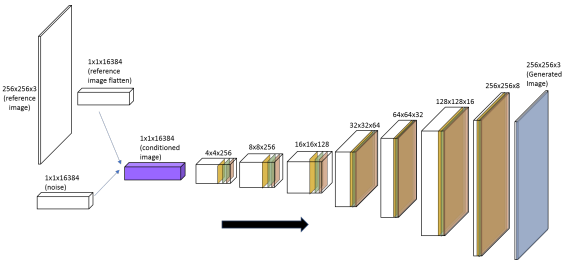

Fig. 6: The architecture of the generator.

This GAN is Conditional and Deep Convolutional network. The generator has an input of a 1 x 1 x 16384 noise tensor which is conditioned with the reference image (the MR image of the patient) via bitwise multiplication. The noise tensor is ran through 256 filters, and a kernel size of 4. The resulting $4 \times 4 \times 256$ tensor is converted to(via another 256 filters) an $8 \times 8 \times 256$ tensor and the kernel size increases by 1. Next the $8 \times 8 \times 256$ tensor is converted to a $16 \times 16 \times 128$ tensor by running it through 64 filters with a kernel size of 3. The resulting $32 \times 32 \times 64$ tensor is ran though 32 filters with a kernel size of three to create a 64 x 64 x 32 tensor. This then goes through 16 filters still a kernel size of 3 to make $128 \times 128 \times 16$ tensor. The resulting $256 \times 256 \times 8$ tensor is ran through 3 filters and a kernel size of 3 to obtain $256 \times 256 \times 3$ image. The tensor representation of the generator can be seen in Fig. 6

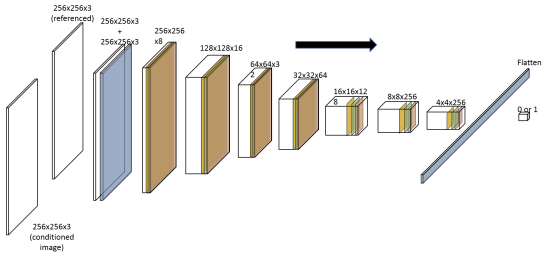

Fig. 7: The architecture of the discriminator.

The discriminator reverses the process with a few exceptions. The conditioned image is added with the reference image and then a sigmoid activation function is applied on the top of it. The discriminator then reverts the $256 \times 256 \times 3$ image all the way, until it the tensor is now a $4 \times 4 \times 256$ tensor. Instead of converting to the noise vector, the $4 \times 4 \times 256$ tensor is flattened and then a 0 or 1 value is given to determine if the generated image fake or real. The discriminator representation of the generator can be seen in Fig. 7

C. Extraction of Cortical Ribbon

After the GAN generates the images, the extraction of the cortical ribbon is needed to get rid of any unnecessary tissue and the skull. In order to do this, we take the following steps. A convex hull is created and then blurred to create a new mask for the brain. The mask is applied to get rid of tissue that is not part of the brain. After this, we convert the grayscale image to an RGB image by adding the 3 RGB channels. We change the image from grayscale to RGB to determine the true blacks inside the skull. Next, we use a yellow flood fill to distinguish between the blacks inside the skull boundary and the blacks outside the skull boundary. A new image is created by layering the matrix to an image with a white background to determine a mask for the image. The mask is then applied to a gray image to isolate the brain itself. Lastly, we conduct a banded threshold from 40 to 60 to isolate the cortical ribbon.

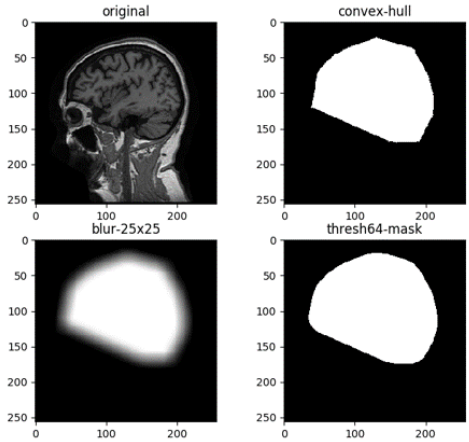

Fig. 8: The extraction of the brain using a convex hull.

D. Use of K-Space

Fig. 5 shows that the fractal dimensions we compute from the patient's current cortical ribbon and the patients predicted cortical ribbon- the generated the MCI images. [12] notes that fractal dimensions of MCI images are slightly lower than that of healthy people. The primary reason is because of the erosion of cortical folds that lead to flattening of gyri and sulci.

Appropriate manipulation of the k-space can produce better contrasts and details of the generated mask. Fig. 10 shows the k-space transformation of cortical ribbons. There are three rows in the figure. The first row has 3 images where the first image is the original image, the second image is k-space, and the third image is the reconstructed image. The

978-1-7281-6926-2/20/$31.00 ©2020 IEEE

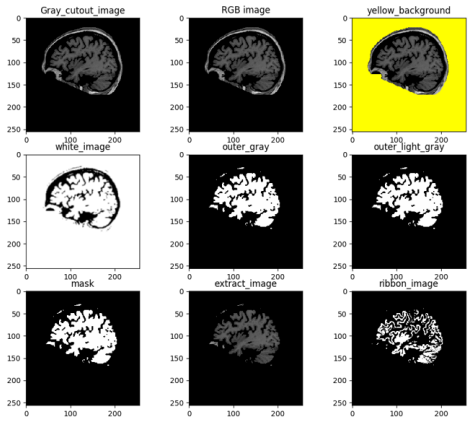

Fig. 9: The process of extracting the brain and cortical ribbon from all other tissues and bone.

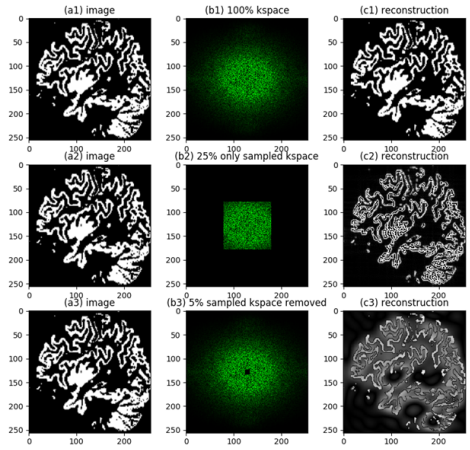

Fig. 10: Appropriate manipulation of the k-space can produce better contrasts and details of the generated mask.

second and third rows have three images where the first image is the original image, like the first row. The second image of the second row is undersampled k-space, where 75% of the frequencies are removed. It is well-known that the reconstructed image that has only low frequencies creates a blurry image during reconstruction. The third row shows the removal of 5% frequencies (lower frequencies) from the center of the k-space, which enhances the outermost edges of the cortical. Furthermore, at the same time, the removal of the lower frequencies sharpens the image. Fig. 10(f), shows that removal of some amount of low frequencies did not eradicate blurring completely, and some degree of blurring is visible. Furthermore, this is removed by thresholding at a higher gray level around 180.

E. Atrophy Prediction

Fig. 16 shows the differences in the relation between the fractal dimension and No-Loss k-space vs. the fractal dimension and Under-sampled k-space. Each data point on both images of Fig. 16 corresponds with the respective image in

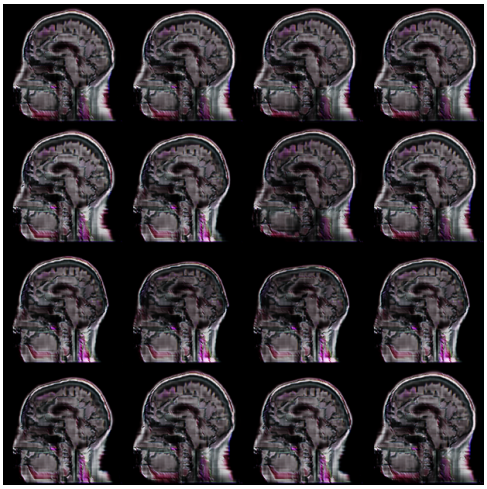

Fig. 11: Results CGDCGAN trained on a conditioned image of MR image with epoch running upto 50000. This is result is from 6^{th} month data.

Fig. 13. Therefore, in Fig. 16a and Fig. 16b, there are 48 points in each. Fig. 16a shows the range of fractal dimension from 1.68 to 1.76. Fig. 16b shows fractal dimension ranges from 1.50 to 1.60. Therefore we see that the No-Loss k-space tends to have a higher fractal dimension whereas the Under-sampled k-space has a lower fractal dimension. Therefore an Under-sampled k-space allows for a clearer and better visualization of the loss of the cortical ribbon.Fig. 19 shows the brain images from Fig. Fig. 11 after the manipulating the full k-space. Fig. 17 averages all the images from Fig. 19 and then takes a threshold of 80 to determine the average cortical ribbon. We chose a threshold of 80 because it gave precise results. There are still many high-frequency noises that need to be removed. We achieve this by under-sampling the k-space. The elimination of many high-frequency noises is evident in Fig. 18. In Fig. 18 we average of all the images in Fig. 20, and then we take a threshold of 80. Comparing Fig. 17 and Fig. 18 we see that Fig. 18 does not contain as much noise (high frequencies) as Fig. 17. Fig. 19 shows the cortical ribbon of the conditioning image with No-loss and Under-sampling. When we overlay the cortical ribbon of the reference imaged with the under-sampled cortical ribbon generated by CDCGAN Fig. 17, we can see the predicted atrophy of the brain. The predicted atrophy can be seen in Fig. 17. The red areas show where the precited atrophy occurs.

Fig. 16 shows the the differences of relation between the fractal dimension and No-Loss k-space vs the fractal dimension and Under-sampled k-space.

Each data point, on both images of Fig. 16 correspond with the respective image in Fig. 13. Therefore, in Fig. 16a and Fig. 16b there are 48 points in each. Fig. 16a shows the range of fractal dimension from 1.68 to 1.76. Fig. 16b shows fractal dimension ranges from 1.50 to 1.60. Therefore we see that the No-Loss k-space tends to have a higher fractal dimension whereas the Under-sampled k-space has a lower

978-1-7281-6926-2/20/$31.00 ©2020 IEEE

fractal dimension. This means that a Under-sampled k-space allows for a clearer and better visualization of the loss of the cortical ribbon. Fig. 19shows the brain images from Fig. 11 after the manipulating the full k-space. Fig. 17 averages all the images from Fig. 19 and then takes a threshold of 80 to determine the average cortical ribbon. A threshold of 80 was chosen because it gave clear results. There is still a lot of high frequency noise that needs to be removed. This is acheived by under-sampling the k-space. This is evident in Fig. 18. Fig. 18 is the average of all the images in Fig. 20 and then taking a threshold of 80. Comparing Fig. 17 and Fig. 18 we see that Fig. 18 is does not contain as much noise(high frequencies) as Fig. 17.

Fig. 19 shows the cortical ribbion of the conditioning image with No-loss and Under-sampling. When the cortical ribbion of the reference imaged is overlayed with the under-sampled cortical ribbon generated by CDCGAN Fig. 17 we are able to see the predicted atrophy of the brain. This can be seen in Fig. 17. The red areas show where the precited atrophy occurs.

V. Experiments

A. Data

In our work, we use MRI data obtained from Alzheimer's Disease NeuroimagingInitiative (ADNI) database [2].

There are three distinct categories in the downloaded data set: 1) Normal controls (NC), mild cognitive impairments (MCI), and Alzheimer's Disease (AD). The data used contains images of patients from several visits within four to five years. Most patients are consistent with their visits, however there are a few who show gaps in their visits. For each patient there are multiple types of MRI images such as MPRAGE and MPR.

We fetch the preprocessed images from ADNI database with the following pipeline descriptions: *MPR; GradWarp; B1 Correction; N3; Scaled* and *MT1; GradWarp; N3m*. These images have different shapes and orientations and contain skull and other organs that need to be removed to accurate performance. We extract the cortical ribbon from the image using the process described in subsection IV-C.

Since we work with scaled images, the RAS+ (Left-Right, Posterior-Anterior, Superior-Inferior) transformation is already encoded in the NIFI transformed data sets. Thus, all brain images have the same orientation. We recomputed all images to 256x256x3 on a single GPU (GTX2080). Gans take a lot of time to generate good images and therefore needs a lot of epochs to run.

In order to predict the MCI-to-AD conversion, we only use MCI and AD images. Normal controls (NC) data is used only to measure the possible loss by comparing it with different stages of MCI. For the stable MCI images, we consider participants that are labeled MCI and have not converged to AD. We know that the cognitive quality of MCI patients drop as they transition to AD. It is always unclear and challenging to measure how or when the patients will transit to the AD.

So, we take visits that are within a five-year-window prediction interval. The total number of stable MCI and AD patients is 532 and 327, respectively. The number of image samples for these two classes are respectively 1764 and 1016.

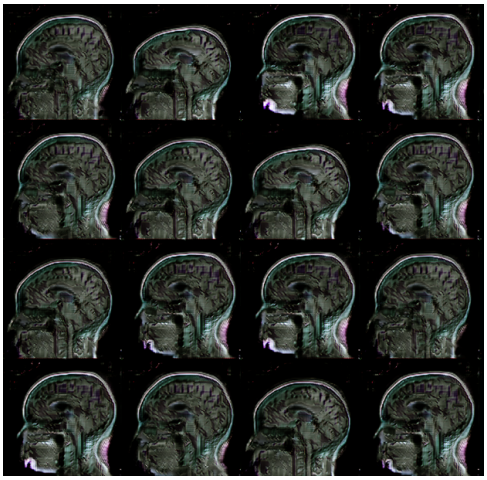

Fig. 12: Results CGDCGAN trained on a conditioned image of MR image with epoch running upto 36000. This is a 12^{th} month data is trained.

Fig. 13: The generated images for the 12 month data after 50 thousand epochs.

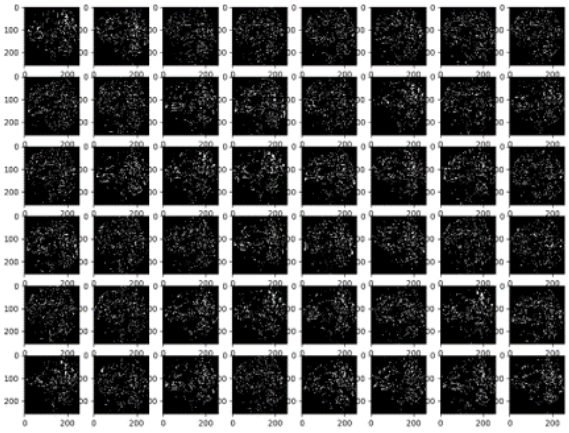

Fig. 14: The generated brain images after the manipulation of the full k-space .

978-1-7281-6926-2/20/$31.00 ©2020 IEEE

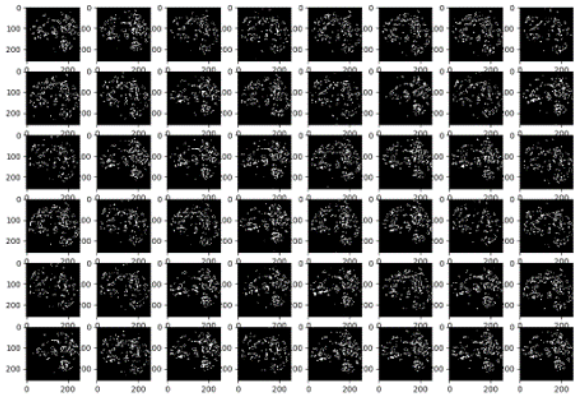

Fig. 15: The generated brain images after the manipulation of the under-sampled k-space .

We categorized the data in 6 visit buckets, starting from 6^{th} month, 12^{th} month, 18^{th} month, 24^{th} month, 36^{th} month, and 48^{th} month.

B. Results from CDCGANs

Fig. 11 shows the generated images of CGDCGAN trained on a conditioned image of MR image after epoch running upto 50000. This is result is based on 6^{th} month data. Fig. 12 shows generated images of CGDCGAN trained on a conditioned image of MR image after epoch running upto 36000. This is result is based on 12^{th} month data. The CDCGAN is implemented in Keras and infrastructure code is written in Python. Training of CDCGANs take a lot of time and GPU memory. With our limited computational setup we were able to train the CDCGAN upto 50000 runs. We also note that the CDCGAN produces a set of sharper images with more training data.

Fig. 21 shows the how the fractal dimension decreases with number of visits starting from 6^{th} month to 48^{th} month. There are four images for each brain slices at 50, 65, 75, and 85. Here we see a decreasing pattern of fractal dimensions with more number of visits. This confirms our observation that fractal dimensions derived from simulated MCI images can be useful.

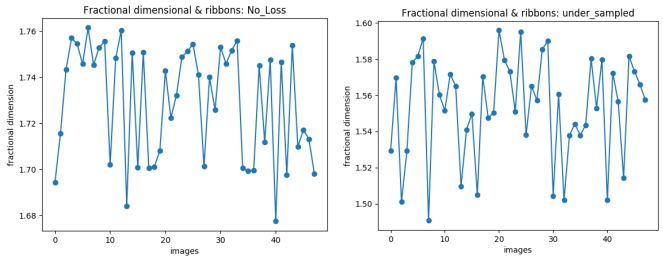

(a) No-Loss (b) Under-Sampled

Fig. 16: The fractal dimension for 48 images.

VI. Conclusion

We proposed a novel approach to simulate the rate of progression of AD and the atrophy of the brain over time. The approach generates synthetic magnetic resonance (MR) images via a cascaded Conditional Deep Convolutional Generative Adversarial Neural Networks (CDCGANs) and then analyze them by computing the fractal dimensionality of the cortical brain ribbons. Our experiments show that it is feasible to predict amount of loss in a quantative way, however, computation realistic images take a long time and intense amount of computing power.

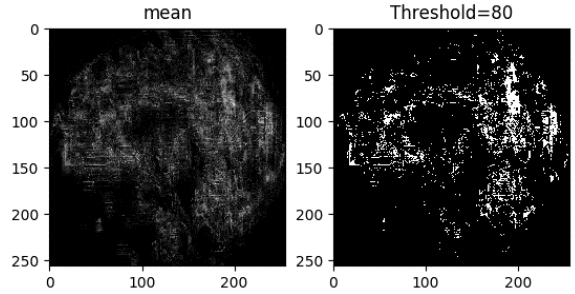

Fig. 17: This is the conversion of the brain given a full k-space.

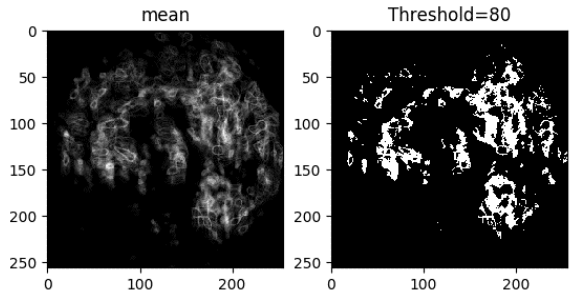

Fig. 18: This is the conversion of the brain given a under-sampled k-space.

References

[1] 2018 Report alzheimer's disease facts and figures. https://www.alz.org/media/documents/alzheimers-facts-and-figures-infographic.pdf. Accessed: 2018.

[2] ADNI: Alzheimer's Disease Neuroimaging Initiative, howpublished = http://adni.loni.usc.edu/, note = Accessed: 2019.

[3] Christopher Bowles, Liang Chen, Ricardo Guerrero, Paul Bentley, Roger N. Gunn, Alexander Hammers, David Alexander Dickie, Maria del C. Valdés Hernández, Joanna M. Wardlaw, and Daniel Rueckert. GAN augmentation: Augmenting training data using generative adversarial networks. *CoRR*, abs/1810.10863, 2018.

[4] Bo Cheng, Daoqiang Zhang, and Dinggang Shen. Domain transfer learning for mci conversion prediction. In Nicholas Ayache, Hervé Delingette, Polina Golland, and Kensaku Mori, editors, *Medical Image Computing and Computer-Assisted Intervention – MICCAI 2012*, pages 82–90, Berlin, Heidelberg, 2012. Springer Berlin Heidelberg.

[5] Youngsang Cho, Joon-Kyung Seong, Yong Jeong, and Sung Yong Shin. Individual subject classification for alzheimer's disease based on incremental learning using a spatial frequency representation of cortical thickness data. *NeuroImage*, 59(3):2217 – 2230, 2012.

[6] M. Frid-Adar, E. Klang, M. Amitai, J. Goldberger, and H. Greenspan. Synthetic data augmentation using gan for improved liver lesion classification. In *2018 IEEE 15th International Symposium on Biomedical Imaging (ISBI 2018)*, pages 289–293, April 2018.

[7] Serge Gauthier, Barry Reisberg, Michael Zaudig, Ronald C Petersen, Karen Ritchie, Karl Broich, Sylvie Belleville, Henry Brodaty, David Bennett, Howard Chertkow, Jeffrey L Cummings, Mony de Leon, Howard Feldman, Mary Ganguli, Harald Hampel, Philip Scheltens,

978-1-7281-6926-2/20/$31.00 ©2020 IEEE

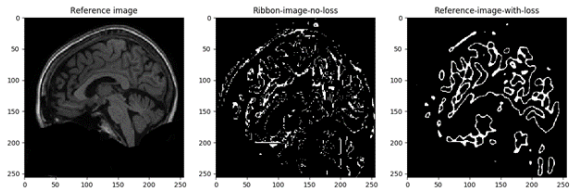

Fig. 19: The generated brain images after the manipulation of the full k-space.

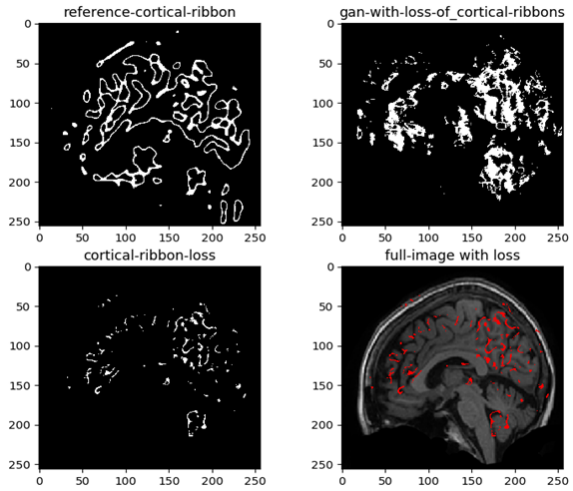

Fig. 20: The generated brain images after the manipulation of the under-sampled k-space. The red areas show predicted loss of matter.

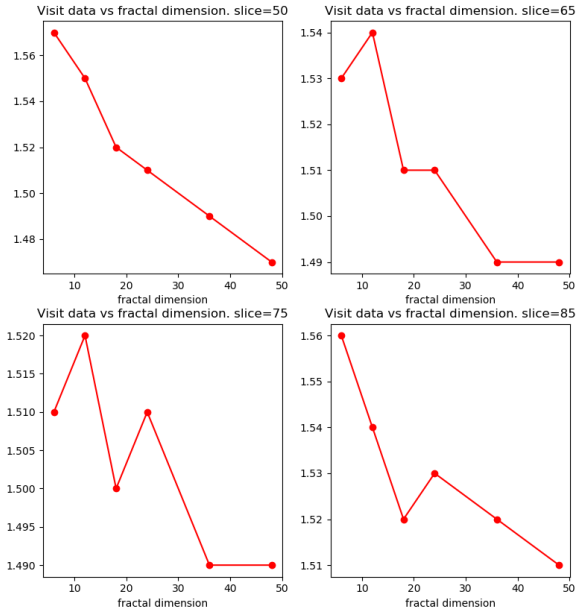

Fig. 21: For different visits the fractal dimension is plotted for different slices.

Mary C Tierney, Peter Whitehouse, and Bengt Winblad. Mild cognitive impairment. *The Lancet*, 367(9518):1262 – 1270, 2006.

[8] Ian J. Goodfellow, Jean Pouget-Abadie, Mehdi Mirza, Bing Xu, David Warde-Farley, Sherjil Ozair, Aaron Courville, and Yoshua Bengio. Generative adversarial nets. In *Proceedings of the 27th International Conference on Neural Information Processing Systems - Volume 2*, NIPS'14, pages 2672–2680, Cambridge, MA, USA, 2014. MIT Press.

[9] C. Han, H. Hayashi, L. Rundo, R. Araki, W. Shimoda, S. Muramatsu, Y. Furukawa, G. Mauri, and H. Nakayama. Gan-based synthetic brain mr image generation. In *2018 IEEE 15th International Symposium on Biomedical Imaging (ISBI 2018)*, pages 734–738, April 2018.

[10] D. Harte. *Multifractals: Theory and Applications*. CRC Press, 2001.

[11] Koshino Kazuhiro, Rudolf A. Werner, Fujio Toriumi, Mehrbod Som Som Javadi, Martin Gilbert Pomper, Lilja B. Solnes, Franco Verde, Takahiro Higuchi, and Steven P. Rowe. Generative adversarial networks for the creation of realistic artificial brain magnetic resonance images. In *Tomography*, 2018.

[12] Brown B. Hwang M. Jeon T. George A. T. King, R. D. and Alzheimer's Disease Neuroimaging Initiative. Fractal dimension analysis of the cortical ribbon in mild alzheimer's disease. *NeuroImage*, 53(2):471–479, 2010.

[13] A. Kruger. Implementation of a fast box-counting algorithm. *Computer Physics Communications*, 98(1):224 – 234, 1996.

[14] J. Langr and V. Bok. *GANs in Action: Deep learning with Generative Adversarial Networks*. Manning Publications, 2019.

[15] Jian Li, Qian Du, and Caixin Sun. An improved box-counting method for image fractal dimension estimation. *Pattern Recognition*, 42(11):2460 – 2469, 2009.

[16] S. Liu, S. Liu, W. Cai, H. Che, S. Pujol, R. Kikinis, D. Feng, M. J. Fulham, and ADNI. Multimodal neuroimaging feature learning for multiclass diagnosis of alzheimer's disease. *IEEE Transactions on Biomedical Engineering*, 62(4):1132–1140, April 2015.

[17] Sidong Liu, Yang Song, Weidong Cai, Sonia Pujol, Ron Kikinis, Xiaogang Wang, and Dagan Feng. Multifold bayesian kernelization in alzheimer's diagnosis. In Kensaku Mori, Ichiro Sakuma, Yoshinobu Sato, Christian Barillot, and Nassir Navab, editors, *Medical Image Computing and Computer-Assisted Intervention – MICCAI 2013*, pages 303–310, Berlin, Heidelberg, 2013. Springer Berlin Heidelberg.

[18] Benoit B Mandelbrot. *The fractal geometry of nature*. Freeman, San Francisco, CA, 1982.

[19] Roy C Martin, Adam Gerstenecker, Kristen L Triebel, Michael Falola, Tarrant McPherson, Gary Cutter, and Daniel C Marson. Declining financial capacity in mild cognitive impairment: A six-year longitudinal study. *Archives of clinical neuropsychology : the official journal of the National Academy of Neuropsychologists*, 34(2):152—161, March 2019.

[20] Mehdi Mirza and Simon Osindero. Conditional generative adversarial nets. *CoRR*, abs/1411.1784, 2014.

[21] Karen Simonyan and Andrew Zisserman. Two-stream convolutional networks for action recognition in videos. In Z. Ghahramani, M. Welling, C. Cortes, N. D. Lawrence, and K. Q. Weinberger, editors, *Advances in Neural Information Processing Systems 27*, pages 568–576. Curran Associates, Inc., 2014.

[22] Daoqiang Zhang, Yaping Wang, Luping Zhou, Hong Yuan, and Dinggang Shen. Multimodal classification of alzheimer's disease and mild cognitive impairment. *NeuroImage*, 55(3):856 – 867, 2011.

[23] J. Zhang, M. Liu, Le An, Y. Gao, and D. Shen. Alzheimer's disease diagnosis using landmark-based features from longitudinal structural mr images. *IEEE Journal of Biomedical and Health Informatics*, 21(6):1607–1616, Nov 2017.

978-1-7281-6926-2/20/$31.00 ©2020 IEEE